Conformational Isomerism and Weak Molecular and Magnetic Interactions in Ternary Copper(II) Complexes of $[Cu(AA)L']ClO_4 \cdot nH_2O$, Where AA = L-Phenylalanine and L-Histidine, L′ = 1,10-Phenanthroline and 2,2-Bipyridine, and n = 1 or 1.5: Synthesis, Single-Crystal X-ray Structures, and Magnetic Resonance Investigations

P. S. Subramanian,[†] E. Suresh,[†] P. Dastidar,[†] S. Waghmode,[‡] and D. Srinivas*[,‡]

Silicate and Catalysis Division, Central Salt & Marine Chemicals Research Institute, Gijubhai Badheka Marg, Bhavnagar 364 002, India, and Catalysis Division, National Chemical Laboratory, Pune 411 008, India

Received February 12, 2001

Weak molecular and magnetic exchange interactions in ternary copper(II) complexes, viz., [Cu(L-phe)(phen)-$(H_2O)]ClO_4$ (**1**), [Cu(L-phe)(bpy)$(H_2O)]ClO_4$ (**2**), and [Cu(L-his)(bpy)$]ClO_4 \cdot 1.5H_2O$ (**3**), where L-phe = L-phenylalanine, L-his = L-histidine, phen = 1,10-phenanthroline, and bpy = 2,2′-bipyridine, have been investigated. Single-crystal X-ray structures reveal that complex **2** crystallizes in a monoclinic space group $P2_1$, with unit cell parameters a = 7.422(7) Å, b = 11.397(5) Å, c = 12.610(2) Å, β = 102.10(5)°, V = 1043.0(11) Å^3, Z = 2, R = 0.0574, and R_w = 0.1657. Complex **3** crystallizes in a monoclinic space group $C2$, with a = 18.834(6) Å, b = 10.563(4) Å, c = 11.039(3) Å, β = 115.23(2)°, V = 1986.6(11) Å^3, Z = 4, R = 0.0466, and R_w = 0.1211. Molecules of **2,** in the solid state, are self-assembled via weak intra- and intermolecular $\pi-\pi$ stacking and H-bonding interactions. Molecules of **3** exhibit intermolecular dimeric association with the Cu···Cu separation being 3.811 Å. X-ray structures and ^{1}H NMR studies reveal conformational isomerism in both solid and liquid states of complexes **1** and **2**. The aromatic side chain of L-phe in **1** and **2** adopts either a "folded" (A) or an "extended" (B) conformation. Variable-temperature ^{1}H NMR and spin lattice relaxation measurements point out interconversion between conformations A and B at temperatures above 323 K. The change in molecular conformation induces a change in the electron density at the site of copper and band gap energy between HOMO and LUMO orbitals. Interestingly, in spite of paramagnetic nature, complexes **1** and **2** are amenable for both EPR and ^{1}H NMR spectroscopic studies. Single-crystal EPR spectra of **2** in three orthogonal planes are consistent with three-dimensional magnetic behavior. Intramolecular exchange dominates the dipolar interactions. The EPR spectra of **3** correspond to weak magnetic interactions between associated dimeric units. The structural and magnetic resonance investigations together reveal that the weak $\pi-\pi$ stacking interactions are the electronic pathways for magnetic interactions in **1**−**3**.

Introduction

Ternary complexes of the type M(AA)L′, where AA = amino acid, L′ = some other ligand or a different amino acid, and M = metal ion, have been receiving considerable interest due to their biological relevance. Sigel et al.[1] have reported that electronic effects such as favorable interactions between π systems, between hydrophobic systems, and between oppositely charged side groups contribute to the stability of the ternary structure. These weak interactions indeed play a crucial role in self-organization of molecules, supramolecular chemistry, and molecular recognition.[2−4] There are many papers describing magnetic interactions in structures of copper(II) complexes mediated via mono- and multiatomic bridged ligands.[5−12] However, studies on complexes wherein the interactions are primarily via weak intermolecular in nature are rather scarce. In such systems EPR spectroscopy is an ideal, complementary technique to study magnetic properties.[13] With this point in view, we report here synthesis and magnetic resonance (single-crystal

* Corresponding author. E-mail: srinivas@cata.ncl.res.in. Fax: (91)-20-5893761.

† Central Salt & Marine Chemicals Research Institute.

‡ National Chemical Laboratory.

(1) Sigel, H. *Angew. Chem., Int. Ed. Engl.* **1975**, *14*, 394. Sigel, H.; Narmann, C. F. *J. Am. Chem. Soc.* **1976**, *98*, 730. Mitchell, P. R.; Sigel, H. *J. Am. Chem. Soc.* **1978**, *100*, 1564.

(2) Lehn, J.-M. *Angew. Chem., Int. Ed. Engl.* **1990**, *29*, 1304.

(3) Desiraju, G. R. *Acc. Chem. Res.* **1996**, *29*, 441. Stang, P. J.; Olenyuk, B. *Acc. Chem. Res.* **1997**, *30*, 502.

(4) Hunter, C. A.; Sanders, J. K. M. *J. Am. Chem. Soc.* **1990**, *112*, 5525. Frieden, E. *J. Chem. Educ.* **1975**, *52*, 754.

(5) *Magneto-Structural Correlations in Exchange Coupled Systems*; Gatteschi, D., Khan, O., Willet, R. D., Eds.; NATO Advanced Study Institute Series; Reidel Publishing Co.: Dordrecht, 1985. Khan, O. *Angew. Chem., Int. Ed. Engl.* **1985**, *24*, 834.

(6) Bencini, A.; Gatteschi, D. *EPR of Exchange Coupled Systems*; Springer-Verlag: Berlin, 1990; Chapter 10.

(7) Strothkamp, K. G.; Lippard, S. J. *Acc. Chem. Res.* **1982**, *15*, 318. Doedens, R. J. *Prog. Inorg. Chem.* **1976**, *21*, 209.

(8) Subramanian, P. S.; Dave, P. C.; Boricha, V. P.; Srinivas, D. *Polyhedron* **1998**, *17*, 443. Subramanian, P. S.; Srinivas, D. *Polyhedron* **1996**, *15*, 985.

(9) van Albada, G. A.; Quiroz-Castro, M. E.; Mutikainen, I.; Turpeinen, U.; Reedjik, J. *Inorg. Chim. Acta* **2000**, *298*, 221.

(10) Papoutsakis, D.; Kirby, J. P.; Jackson, J. E.; Nocara, D. *Chem.—Eur. J.* **1999**, *5*, 1474.

(11) Balagopalakrishna, C.; Rejasekharan, M. V. *Phys. Rev. B* **1990**, *42*, 7794.

(12) Subramanian, P. S.; Suresh, E.; Srinivas, D. *Inorg. Chem.* **2000**, *39*, 2053.

(13) Bencini, A.; Benelli, C.; Gatteschi, D.; Znachini, C. *Proc.—Indian Acad. Sci., Chem. Sci.* **1987**, *98*, 13.

10.1021/ic010182d CCC: $20.00
Published on Web 07/10/2001

EPR and ^{1}H NMR) spectroscopic studies of [Cu(L-phe)(phen)-(H_2O)]ClO_4 (**1**), [Cu(L-phe)(bpy)(H_2O)]ClO_4 (**2**), and [Cu(L-his)(bpy)]$ClO_4 \cdot 1.5H_2O$ (**3**) complexes. Single-crystal X-ray structures of **2** and **3** are also reported. The L-phe ligand exhibits conformational isomerism. The aromatic side chain of L-phe adopts "folded" (A) and "extended" (B) conformations. Single-crystal X-ray structure reveals that complex **2** in the present study crystallizes with the former (A) conformation. The crystal structure of **2** with the latter (B) conformation was reported earlier by Sugimori et al.[14] Such a conformational isomerism was also observed by Marcelli et al.[15] in the structure of bis-(L-phenylalaninamidato)copper(II) complex.

Copper(II) complexes are usually not amenable for ^{1}H NMR study due to paramagnetism and unfavorable relaxation times. Interestingly, complexes **1** and **2** could be studied by both EPR and ^{1}H NMR studies. Single-crystal EPR spectra of **2** showed an exchange-narrowed signal. Comparative structural and EPR studies indicate that the weak $\pi-\pi$ stacking and H-bonding interactions are the pathways for the intermolecular magnetic exchange interactions. Variable-temperature ^{1}H NMR studies in D_2O solutions and ^{1}H spin lattice relaxation measurements revealed conformational dynamics of the aromatic side chain of the L-phe ligand at higher temperatures. Molecular modeling studies on **2** complemented the experimental results. The noteworthy results of the present study are (i) conformational dynamics of the coordinated L-phe ligand, (ii) feasibility of the paramagnetic copper(II) complexes for both EPR and NMR studies, and (iii) magnetism primarily via weak intermolecular interactions ($\pi-\pi$ stacking) since the closest Cu−Cu distance is 3.81 Å in complex **3**. In fact these properties are responsible for the highly selective and cooperative activity of metalloenzymes in redox transformations. The consequences of conformational changes on the spectra and electronic properties are investigated.

Experimental Section

Materials. $CuSO_4 \cdot 5H_2O$, L-phe, L-his, phen, bpy, and $NaClO_4$ were obtained from Aldrich Co. The solvents were of A.R. grade and purified further by standard procedures.[16]

Synthesis of [Cu(L-phe)(phen)(H_2O)]ClO_4 (1). A mixture of L-phe (0.826 g, 5 mmol) and NaOH (0.2 g, 5 mmol) dissolved in 10 mL of distilled water was added to an aqueous solution (25 mL) of $CuSO_4 \cdot 5H_2O$ (1.248 g, 5 mmol) with stirring for 30 min. Then phen (0.941 g, 5 mmol) dissolved in 10 mL of ethanol was added. The solution was stirred for another 2 h with heating at 333 K. At the end of the reaction, $NaClO_4$ (0.7 g) dissolved in distilled water was added. Slow evaporation of the reaction mixture at 298 K yielded dark blue, needle-shaped crystals in 8−10 days. Anal. Calcd for $CuC_{21}N_3H_{20}ClO_7$: C, 48.00; H, 3.81; N, 8.10. Found: C, 48.81; H, 3.91; N, 7.68. FT-IR data (cm^{-1}): ν(O−H/C−H/N−H) 3452, 3333, 3028; $\nu(COO^-)$ 1622, 1238; ν(C═N, C═C) 1589, 1519; $\nu(ClO_4^-)$ 1154, 1121, 1109, 1088, 1033.

Synthesis of [Cu(L-phe)(bpy)(H_2O)]ClO_4 (2). Complex **2** was prepared as described above except that bpy (0.821 g, 5 mmol) was used in place of the phen ligand. Slow evaporation of the reaction mixture yielded good quality dark blue, platelike crystals in about a week. Anal. Calcd for $CuC_{19}N_3H_{20}ClO_7$: C, 45.51; H, 3.99; N, 8.38. Found: C, 46.72; H, 3.69; N, 8.60. FT-IR data (cm^{-1}): ν(O−H/C−H/N−H) 3450, 3113, 2891; $\nu(COO^-)$ 1651, 1267; ν(C═N, C═C) 1605, 1525; $\nu(ClO_4^-)$ 1144, 1121, 1109, 1088, 1033.

Synthesis of [Cu(L-his)(bpy)]$ClO_4 \cdot 1.5H_2O$ (3). Complex **3** was prepared in a manner similar to that of **2** except that L-his (0.771 g, 5 mmol) was used in place of the L-phe ligand. Good quality, needle-shaped, blue crystals were obtained by slow evaporation of the reaction mixture. Anal. Calcd for $CuC_{16}N_5H_{19}ClO_{7.5}$: C, 38.40; H, 3.80; N, 14.00. Found: C, 38.37; H, 3.80; N, 14.15. FT-IR data (cm^{-1}): ν(O−H/C−H/N−H) 3450−3026; $\nu(COO^-)$ 1620, 1253; ν(C═N, C═C) 1576, 1525; $\nu(ClO_4^-)$ 1142, 1120, 1109, 1092, 1034.

CAUTION! Perchlorate salts of metal complexes are potentially explosive and should be handled with great care.

Physical Measurements. Microanalysis of the complexes was done by using a Perkin-Elmer PE 2400 series II CHNS/O elemental analyzer. FT-IR spectra for KBr pellets (1% w/w) were recorded on a Shimadzu FT-COM 1 spectrophotometer. Electronic spectra were recorded in several solvents using Shimadzu (UV-160A) and HP diode array (model 8452 A) UV−visible spectrometers. EPR investigations were carried out on a Bruker EMX X-band spectrometer operating at a field modulation of 100 kHz, modulation amplitude of 2 G, and microwave radiation power of 2 mW. Measurements at 77 K were done using a quartz finger Dewar. Only complex **2** yielded suitable quality single crystals for EPR measurements. Single-crystal EPR measurements were performed in three orthogonal planes, at 10° intervals, and spectral simulations were done by using the Bruker Simfonia software package.

^{1}H NMR spectra of the complexes in D_2O were recorded on a Bruker 200 MHz DPX Avance FT-NMR spectrometer. TMS was used as an internal standard. Prior to NMR measurements the dissolved oxygen was removed by purging the sample solutions with zero-grade nitrogen gas. ^{1}H spin lattice relaxation time (T_1) measurements were done by using the Bruker XWIN NMR software package and the inversion recovery technique consisting of the following train of pulse sequences:[17]

$$(180° - \tau - 90° - \mathrm{Aq} - D)_n$$

Here Aq is the acquisition time, D is the delay to allow equilibrium to be reached and 8.9 μs is the calibrated 90° pulse. The values of magnetization, directly proportional to NMR signal intensity, vary from $-M_z(0)$ (when $\tau = 0$) to $M_z(\infty)$ (when $\tau = 5T_1$); τ is the variable time delay between the two pulses. The magnetization relates to T_1 by the following equation:

$$M_z(\tau) = M_z(\infty)[1 - 2\exp(-\tau/T_1)] \quad (1)$$

T_1 can be calculated by a least-squares analysis of the experimental magnetization data as a function of τ.

X-ray Crystallographic Analysis. Single-crystal X-ray data of complexes **2** and **3** were collected on an Enraf-Nonius CAD-4 diffractometer with graphite-monochromatized Mo Kα radiation (λ = 0.7107 Å). Unit cell parameters and orientation matrices of **2** and **3** were obtained from least squares refinements using 25 reflections within the θ range 8−12°. The $\omega-2\theta$ scan mode with maximum θ value being 24.93° was used to collect the intensity data for both of the complexes. Preliminary data, cell refinement, and intensity data collection were carried out using the program CAD4-PC.[18] The data reduction was done using NRCVAX.[19] The data were corrected for Lorentz and polarization effects but not for absorption. Structure solution was carried out using the Patterson method with full-matrix least squares refinement on F^2 using SHELXL-97.[20] Scattering factors and anomalous dispersion were taken from the *International Tables for X-ray Crystallography*.[21]

In the case of complex **3**, the ClO_4^- ion was found disordered. After complete convergence of all of the non-hydrogen atoms of the complex cation, perchlorate ion was located from the difference Fourier map. The peak height of Cl was ~16 e Å^{-3}, and eight peaks attached to the

(14) Sugimori, T.; Masuda, H.; Ohata, N.; Koiwai, K.; Odani, A.; Yamauchi, O. *Inorg. Chem.* **1997**, *36*, 576.
(15) Marchelli, R.; Dossena, A.; Casnati, G.; Fava, G. G.; Ferrari, M. *J. Chem. Soc., Chem. Commun.* **1985**, 1672.
(16) Perrin, D. D.; Armarego, W. L. F.; Perrin, D. R. *Purification of Laboratory Chemicals*; Pergamon Press: Oxford, 1980.
(17) Beckman, E. D. *High-Resolution NMR*; Academic Press: New York, 1969.
(18) *CAD-4 PC Software*, Version 5; Enraf-Nonius: Delft, The Netherlands, 1989.
(19) Gabe, E. I.; Le Page, Y.; Charland, I. P.; Lee, F. L.; White, P. S. *J. Appl. Crystallogr.* **1989**, *22*, 384.
(20) Sheldrick, G. M. *SHELXL-97, Program for the Solution of Crystal Structures*; University of Göttingen: Göttingen, Germany, 1997.
(21) *International Tables for X-ray Crystallography*; Kynoch Press: Birmingham, 1974; Vol. IV.

Table 1. Summary of Crystallographic Data for $[Cu(L\text{-phe})(bpy)(H_2O)]ClO_4$ (**2**) and $[Cu(L\text{-his})(bpy)]ClO_4 \cdot 1.5H_2O$ (**3**)

	complex **2**	complex **3**
chem formula	$C_{19}H_{20}N_3O_7ClCu$	$C_{16}H_{19}N_5O_{7.5}ClCu$
fw	500.36	500.35
a (Å)	7.422(7)	18.834(6)
b (Å)	11.397(5)	10.563(4)
c (Å)	12.610(2)	11.039(3)
α (deg)	90.00	90.00
β (deg)	102.10(5)	115.23(2)
γ (deg)	90.00	90.00
V (Å^3)	1043.0(11)	1986.6(11)
Z	2	4
cryst syst	monoclinic	monoclinic
space group	$P2_1$ (No. 4)	*C*2 (No. 5)
T (K)	296	296
λ (Å)	0.7107	0.7107
ρ_{calcd} (g cm^{-3})	1.593	1.673
μ (cm^{-1})	8.98	12.88
$R(F_o^2)^a$	0.0574	0.0466
R_w $(F_o^2)^a$	0.1657	0.1211

^{a} $R = \sum||F_o| - |F_c||/\sum|F_o|$; $R_w = [\sum w(F_o^2 - F_c^2)^2]/\sum[w(F_o^2)^2]^{1/2}$; $w = 1/\sigma(F_o)^2$.

Cl atom with peak heights ranging from 1.2 to 3.8 e Å^{-3} corresponded to disordered oxygen atoms; the Cl atom of the disordered perchlorate anion was refined anisotropically; the occupancy factor for the attached disordered oxygen atoms was assigned depending on the peak heights. Inclusion of all of these eight atoms, corresponding to two orientations of the ClO_4^- ion, improved significantly the refinement parameters (*R*, R_w, and goodness of fit) implying the right assignment of anion disorder.

Hydrogen atoms were either located from the difference Fourier map or kept fixed using the riding model, except for water hydrogens in complex **2**, which were not available from the difference Fourier map. In the case of complex **3** all of the hydrogen atoms were kept fixed during refinement. Crystallographic data and refinements for both of the complexes are presented in Table 1.

Molecular Modeling and DFT Calculations: Methodology. Different molecular conformations of complex **2** were generated by systematically varying the dihedral angles C11−C12−C13−C14 and C12−C13−C14−C15 between 0° and 360°, in steps of 20°. The single-point strain energies of these clusters were calculated using the MMFF94 basis set. MO energies and electron density distributions were evaluated by the DFT method using the STO DN** basis set. All of the computations were carried out on a Silicon Graphics O_2 workstation using the SPARTAN and MSI software packages.

Results

X-ray Structure, Conformational Geometry, and Molecular Association: $[Cu(L\text{-phe})(bpy)(H_2O)]ClO_4$ (2). An ORTEP[22] view of complex cation **2** along with the atom-numbering scheme is shown in Figure 1a. Selected bond distances and angles are listed in Table 2. Copper possesses a distorted square pyramidal geometry, and L-phe coordinates through amino nitrogen and deprotonated carboxylato oxygen atoms. The ligands bpy (Cu1−N1 = 1.987(9) Å, Cu1−N2 = 2.002(8) Å) and L-phe (Cu1−N3 = 2.028(8) Å, Cu−O1 = 1.946(7) Å) form the square base, while the water molecule makes a long axial coordination (Cu1−O1W = 2.298(7) Å). The square base formed by the coordinating atoms is almost planar with a maximum deviation of 0.053 Å, and the Cu1 atom is out of the best plane of N1N2N3O1 by 0.220 Å toward the axial water molecule. The dihedral angle between the planes CuN1N2 and CuN3O1 is 17.40(5)°.

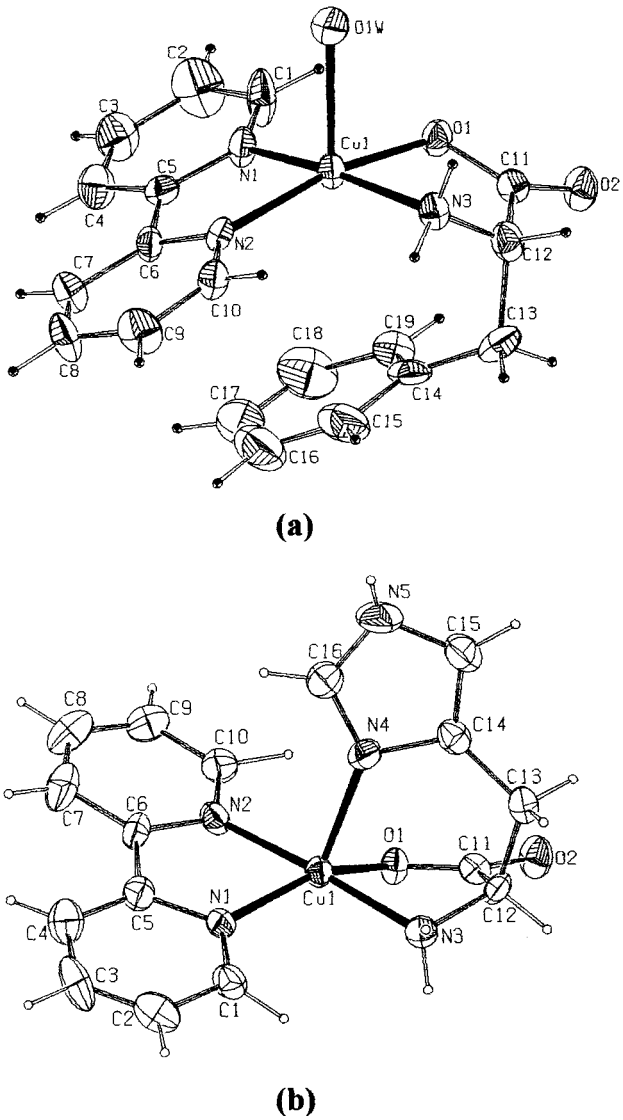

Figure 1. ORTEP views of (a) $[Cu(L\text{-phe})(bpy)(H_2O)]ClO_4$ (**2**) and (b) $[Cu(L\text{-his})(bpy)]ClO_4 \cdot H_2O$ (**3**).

In related mixed ligand copper complexes the aromatic side chain of L-phe exhibited different orientations with respect to the metal coordination plane.[14,23] The aromatic side chain adopts an "extended" conformation and the phenyl group orients perpendicular to the coordination square plane in structures $[Cu(L\text{-phe})(phen)Cl] \cdot 3H_2O$[14] and $[Cu(L\text{-}o\text{-Me-phe})(phen)(H_2O)]ClO_4$.[23] On the contrary, the side chain takes up a "folded" geometry with the phenyl group orienting parallel to the coordination square plane in structures $[Cu(L\text{-}NH_2Phe)(bpy)]NO_3 \cdot H_2O$ and $[Cu(L\text{-Tyr})(phen)(H_2O)]\ ClO_4 \cdot 1.5H_2O$.[14] L-Phe in complex **2** adopts the "folded" conformation. The phenyl ring is almost parallel to the bpy moiety (Figure 1a) with a tilt angle of 6.82(5)°. Complex **2** exhibits both intra- and intermolecular $\pi-\pi$ stacking interactions between the phenyl and bpy rings (Figure 2). The intramolecular stacking distance between centroids C3G of the phenyl ring (C14 to C19) and C2G of bpy (N2C6 to C10) is 3.84(1) Å. The distances between centroid C3G and the nearest bpy atoms N2 and C6 are 3.43(4) and 3.54(2) Å, respectively. A significant deviation of the C_α carbon atom (C12) from the coordination plane toward the phenyl ring

(22) Johnson, C. K. ORTEP. Report ORNL-3794; Oak Ridge National Laboratory: Oak Ridge, TN, 1976.

(23) Mizutani, S.; Toviosue, H.; Kiuosluta, K.; Jitsukana, K.; Masuda, H.; Einega, H. *Bull. Chem. Soc. Jpn.* **1999**, *72*, 981.

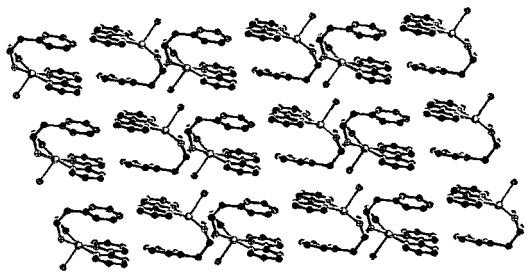

Figure 2. Pluton diagram showing the intra- and intermolecular $\pi-\pi$ stacking interactions of aromatic groups in [Cu(L-phe)(bpy)(H_2O)]ClO_4 (**2**). Perchlorate anions are omitted for clarity.

Table 2. Selected Bond Lengths (Å) and Bond Angles (deg) of Cu(L-phe)(bpy)(H_2O)]ClO_4 (**2**) and [Cu(L-his)(bpy)]ClO_4·1.5H_2O (**3**)

[Cu(L-phe)(bpy)(H_2O)]ClO_4 **2**			
Cu1−O1	1.946(7)	Cu1−N1	1.987(9)
Cu1−N2	2.002(8)	Cu1−N3	2.028(8)
Cu−O1W	2.298(7)		
O1−Cu1−N1	92.3(3)	O1−Cu1−N2	163.3(3)
N1−Cu1−N2	80.8(3)	O1−Cu1−N3	81.5(2)
N1−Cu1−N3	169.2(4)	N2−Cu1−N3	102.7(4)
O1−Cu1−O1W	90.5	N1−Cu1−O1W	97.8(3)
N2−Cu1−O1W	105.5(3)	N3−Cu1−O1W	91.1(3)
C1−N1−Cu1	124.3(8)	C5−N1−Cu1	114.6(7)
C6−N2−Cu1	114.9(7)	C10−N2−Cu1	127.5(7)
C11−O1−Cu1	114.6(6)	C12−N3−Cu1	105.9(6)
[Cu(L-his)(bpy)]ClO_4·1.5H_2O (**3**)			
Cu1−O1	1.995(5)	Cu1−N1	2.028(6)
Cu1−N2	2.007(6)	Cu1−N3	1.962(7)
Cu1−N4	2.114(6)		
N3−Cu1−O1	83.0(2)	N3−Cu1−N2	174.5(3)
O1−Cu1−N2	93.4(2)	N3−Cu1−N1	100.9(3)
O1−Cu1−N1	153.2(2)	N2−Cu1−N1	80.5(2)
N3−Cu1−N4	88.5(3)	O1−Cu1−N4	95.7(3)
N2−Cu1−N4	96.0(3)	N1−Cu1−N4	110.8(3)
C1−N1−Cu1	126.5(5)	C12−N3−Cu1	104.2(4)
C5−N1−Cu1	115.3(5)	C16−N4−Cu1	131.5(6)
C14−N4−Cu1	122.7(5)	C10−N2−Cu1	124.9(6)
C6−N2−Cu1	115.0(5)	C11−O1−Cu1	111.0(5)

(0.85 Å) together with a low angle between the mean planes N1N2N3O1 and C14 to C19 (17.02(4)°) perhaps makes the "folded" geometry possible. Cu(II) makes close contacts with aromatic carbon atoms C14 and C19 of the L-phe ligand (Cu···C14 = 3.19(6) Å and Cu···C19 = 3.34(8) Å). Complex **2** also exhibits intermolecular stacking interactions through the phenyl ring of L-phe of one molecule and bpy of the neighboring molecule (Figure 2). The distance between centroids C3G and C2GA is 4.03(6) Å. Here, C2GA is the centroid of the bpy ring of the adjacent molecule, containing atoms N2A and C6A to C10A. The closest distance between carbon atom C7A, which is part of the staggered bpy ring of the adjacent molecule, and C3G is 3.47(6) Å.

Earlier Sugumorai et al.[14] reported the X-ray structure of another crystalline form of complex **2**. In their structure[14] the asymmetric unit contained two identical molecules and the phenyl ring of L-phe had an "extended" conformation, different from that observed in the present structure. The molecule exhibited intermolecular stacking interactions between the bpy units of adjacent molecules, but no intramolecular interactions were noticed. A combination of coordination and weak intra/intermolecular $\pi-\pi$ stacking interactions are responsible for the supramolecular architecture of complex **2** in the present structure, in the solid state.

The complex makes N−H···O and C−H···O contacts between the screw-related molecules. Both of the amino hydrogens (H1N3 and H2N3) of L-phe are involved in intermolecular N−H···O hydrogen bonding with perchlorate oxygen O6 and uncoordinated carboxylato oxygen O2, respectively. The ligand bpy makes C−H···O interactions with the perchlorate oxygen O5 and the uncoordinated carboxylato oxygen O2. These H-bonding interactions run along the *b*-axis in layers between the screw-related molecules. The various H-bonding interactions are as follows:

D−H···A*	D−H (Å)	H···A (Å)	D···A (Å)	∠D−H···A (deg)
N3−H1···O6[1]	0.90(1)	2.48(1)	3.14(1)	131.2(2)
N3−H2···O2[2]	0.90(1)	2.25(1)	3.03(1)	145.0(3)
C7−H7···O5[3]	0.93(1)	2.426(1)	3.321(3)	161.3(7)
C10−H10···O2[2]	0.93(1)	2.317(1)	3.227(3)	166.0(1)

*Symmetry code (superscript): 1 = *x*, *y*, −1 + *z*; 2 = 1 − *x*, $^1/_2$ + *y*, −*z*; 3 = *x*, *y*, *z*.

The C−H···O interactions are much stronger than the N−H···O interactions. Even though it was not possible to locate the H atoms of the coordinated water molecule, O1W is making good short contacts, along the *b*-axis, with the carboxylato (O1W··· O2 = 2.83(1) Å) and perchlorate oxygen atoms (O1W···O6 = 2.88(4) Å).

The nearest intermolecular Cu···Cu distance is 7.14(3) Å, and its direction is along the diagonal of the *ac*-plane. The same Cu center is separated by 7.35(2) and 7.42(2) Å, respectively, from the 2_1 screw related molecules, and these Cu···Cu directions are aligned along the *a*-axis in the solid state packing. The weak intermolecular stacking and H-bonding interactions are the causes for three-dimensional magnetic behavior of **2** in the solid state (vide infra).

[Cu(L-his)(bpy)]ClO_4·1.5H_2O (3). The perspective view of complex cation **3** with the atom-numbering scheme is shown in Figure 1b. The selected bond distances and angles are listed in Table 2. As in **2,** copper(II) ion in complex **3** also possesses a distorted square pyramidal geometry. The basal plane is defined by the coordinating nitrogen atoms of bpy ligand (Cu1−N1 = 2.028(6) Å and Cu1−N2 = 2.007(6) Å) and α-amino nitrogen (N3) and α-carboxylato oxygen (O1) of L-his ligand (Cu1−N3 = 1.962(7) Å, Cu1−O1 = 1.995(5) Å). The fifth coordination is provided by imidazole ring nitrogen N4 of L-his. The Cu1−N4 bond is comparatively longer than the other Cu−N bonds (Table 2). The square base formed by coordinating N1, N2, N3, and O1 atoms shows a maximum deviation of 0.192 Å from planarity and a tetrahedral bias (Table 2). Copper is out of the best plane by 0.271 Å toward the axially coordinated imidazole nitrogen N4 of L-his.

Crystal packing reveals that cations of adjacent molecules are arranged in dimeric association (Figure 3). These pairs are held together by $\pi-\pi$ stacking interactions between the pyridyl rings of coordinated bpy ligands. The intermolecular Cu1··· Cu1A separation in the associated pair is 3.811 Å, and the stacking distance is 3.66(4) Å. Pyridyl rings of the stacked pairs are almost planar, with a slight twist of 2.83°. The strong $\pi-\pi$ stacking interaction of bpy ligands in the solid state is the driving force for closer approach of metal centers.

Molecule **3** is involved in extensive hydrogen-bonding (N−H···O, O−H···O, C−H···O, O−H···N) interactions involving imidazole nitrogen, carboxylato oxygens, distorted perchlorato oxygens, lattice water molecules, and bpy, which in turn stabilize the molecule in the crystal lattice. The lattice water molecule is far away from the metal center with Cu1···O1W = 5.35 Å.

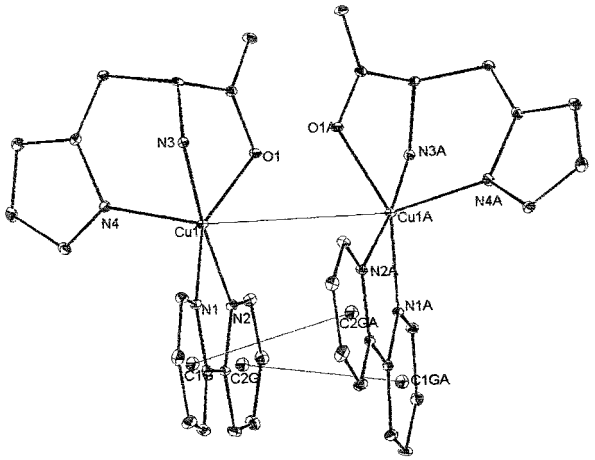

Figure 3. Intermolecular dimeric association $\pi-\pi$ stacking interactions between bpy ligands in [Cu(L-his)(bpy)]ClO_4·1.5 H_2O (**3**). The centroids of bpy rings C1G, C2G, C1GA and C2GA are indicated.

The various H-bonding interactions with symmetry code are as follows:

D−H···A*	D−H (Å)	H···A (Å)	D···A (Å)	∠D−H···A (deg)
N5−H5N···O1W[1]	0.68(1)	2.321(1)	2.938(2)	152.10(2)
O2W−H1O2···O2[2]	1.10(2)	1.722(2)	2.781(2)	160.86(3)
N3−H13N···O3[3]	1.086(3)	2.006(2)	3.018(3)	153.8(2)
O2W−H2O2···N3[4]	1.114(3)	2.437(2)	3.5057(3)	159.99(2)
N3−H2N3···O1[5]	0.938(1)	2.219(2)	3.3032(3)	144.98(4)
C1−H1···O5[6]	1.003(1)	2.477(3)	3.469(3)	170.25(2)
C3−H3···O2W[7]	0.930(1)	2.493(4)	3.379(2)	159.23(2)
C4−H4···O2[8]	0.930(2)	2.549(2)	3.470(2)	170.88(2)
C7−H7···O2[8]	0.930(3)	2.517(2)	3.413(3)	161.8(3)
C15−H15···O6[9]	0.930(2)	2.550(2)	3.377(3)	148.34(2)
C13−H131···O3[3]	0.970(2)	2.556(2)	3.324(3)	136.18(3)

*Symmetry code (superscript): $1 = {}^1/_2 + x, -{}^1/_2 + y, z$; $2 = {}^1/_2 - x, {}^1/_2 + y, z$; $3 = {}^1/_2 - x, -{}^1/_2 + y, 1 - z$; $4 = {}^1/_2 + x, {}^1/_2 + y, z$; $5 = -x, y, -z$; $6 = -{}^1/_2 + x, -{}^1/_2 + y, z$; $7 = -{}^1/_2 + x, {}^1/_2 + y, z$; $8 = x, 1 + y, z$; $9 = x, -1 + y, z$.

Electronic Spectra. Complexes **1**−**3** were soluble in several solvents and showed moderately intense transitions of ligand origin in the range 260−318 nm and a broad asymmetric band corresponding to d−d transitions in the range 580−690 nm. The d−d band for **1** and **2** undergoes a red shift in different solvents in the order THF > pyridine > DMF ≥ H_2O ≥ DMSO ≥ CH_3OH > $(CH_3)_2CO$ > CH_3CN, attributable to solvent coordination or solvolysis. This band for **3** is invariant in CH_3CN, $(CH_3)_2CO$, DMF, DMSO, and pyridine solvents, but it exhibits a red shift in CH_3OH and THF from 640 to 696 nm. The spectral data (Table 3) are consistent with an octahedral geometry for **3** in CH_3OH and THF.[24] The geometry of **3**, in the rest of the solvents, is square pyramidal, as observed in the solid state. Complexes **1** and **2**, on the other hand, are square planar in CH_3CN and $(CH_3)_2CO$, square pyramidal in CH_3OH, H_2O, DMF, DMSO, and pyridine, and octahedral in THF. Complexes **1** and **2** showed an additional weak shoulder around 337 nm attributable to a charge transfer transition from the HOMO(bpy/phen) to LUMO(L-phe) π-orbitals.

EPR Spectra. Polycrystals of **1** and **2** showed similar EPR spectra, at 298 and 77 K, characteristic of axial **g** tensors (Figure 4a,b). The copper hyperfine features could not be resolved due to intermolecular interactions in the solid state. Complex **3**, on the other hand, showed an isotropic signal at $g_{av} = 2.122$ (Figure 4c). Additional, weak signals appeared at high spectrometer gain (Figure 4c,d) as shoulders (on either side of the strong isotropic signal) at 2790 and 3515 G and as a well-separated signal at 1625 G. These signals are consistent with weak dimeric intermolecular association in the solid state.

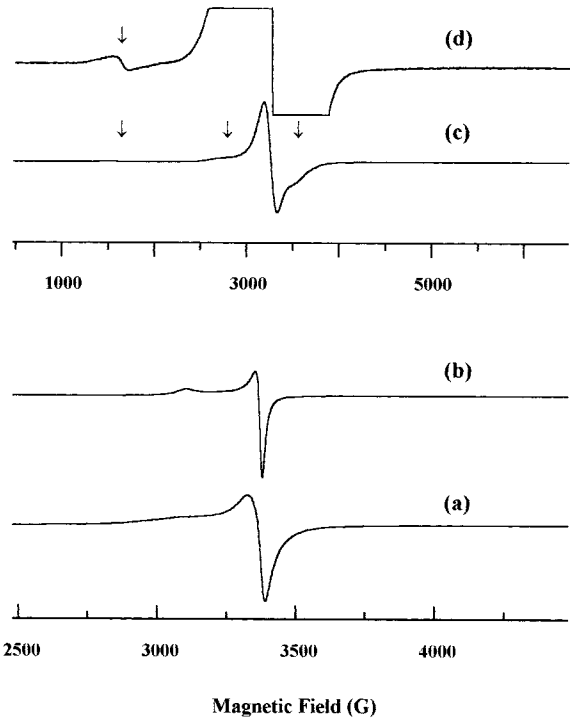

Figure 4. X-band EPR spectra at 298 K of polycrystalline samples: [Cu(L-phe)(phen)(H_2O)]ClO_4 (**1**), (b) [Cu(L-phe)(bpy)(H_2O)]ClO_4 (**2**), and (c) [Cu(L-his)(bpy)]ClO_4·1.5H_2O (**3**). (d) The same as for spectrum c except at higher spectrometer gain. Arrows indicate the signals corresponding to dimeric molecular association in **3**.

EPR spectra for the single crystals of **2** were recorded by rotating the crystals in three orthogonal planes. Although there are two molecules in a unit cell, these are magnetically equivalent and showed a single resonance at all the crystal orientations. The g parameters at different orientations were fitted to the following $\mathbf{g}^2$ tensor expression:

$$g^2(i) = \alpha_i + \beta_i \cos 2\theta + \gamma_i \sin 2\theta \qquad (2)$$

where $g^2(i)$ is the g value in the ith crystal rotation and θ is the azimuthal angle of the magnetic field. The angular variations of g in all three planes are shown in Figure 5. The g anisotropy is larger in plane III than in planes I and II. The components of the **g** tensor were estimated as described earlier.[12] The **g** tensor has rhombic symmetry with $g_x = 2.059$, $g_y = 2.056$, and $g_z = 2.235$. Figure 6 shows the variation of line width (ΔH_{pp}) as a function of crystal orientation in all three orthogonal planes. A maximum ΔH_{pp} of 51.6 G and a minimum of 16.4 G was observed in plane III. Variation of ΔH_{pp} is smaller in planes I and II. The line shape is more toward Gaussian with the Lorentzian/Gaussian ratio being 0.09. In general, in pure paramagnetic solids, the line width has contributions from both dipolar and exchange interactions. The former broadens while the latter narrows the EPR signal. In three-dimensional magnetic systems the latter interaction dominates and the signals are exchange narrowed. However, in low-dimensional systems the exchange effects are less effective and the line widths are between the exchange-narrowed and dipolar broadened limits. For a Cu···Cu separation of 7−7.5 Å, one should observe a

(24) Hathaway, B. J. In *Comprehensive Coordination Chemistry*; Wilkinson, G., Gillard, R. D., McCleverty, J. A., Eds.; Pergamon: Oxford, 1987; Vol. 5, Chapter 53, p 558.

Table 3. UV−Vis Data for [Cu(L-phe)(phen)(H_2O)]ClO_4 (**1**), [Cu(L-phe)(bpy)(H_2O)]ClO_4 (**2**), and [Cu(L-his)(bpy)]ClO_4·1.5H_2O (**3**) in Different Solvents

	λ (ϵ); nm (M^{-1} cm^{-1})		
solvent	**1**	**2**	**3**
CH_3CN	299 (3764), 599 (46)	268 (2543), 306 (2850), 582 (112)	266 (2605), 644 (67)
$(CH_3)_2CO$		330 (1305), 590 (81)	328 (802), 642 (90)
CH_3OH	299 (3653), 612 (24)	268 (2724), 304 (3004), 610 (62)	266 (2670), 304 (2933), 316 (2967), 694 (102)
H_2O	262 (1005), 304 (1568), 620 (8)	260 (2316), 304 (2497), 618 (60)	260 (2873), 308 (3117), 672 (83)
DMSO	304 (2103), 612 (22)	312 (2641), 618 (75)	306 (3132), 320 (3179), 640 (112)
DMF	302 (1791), 610 (22)	278 (2281), 306 (2887), 620 (69)	316 (2563), 646 (95)
pyridine	305 (2058), 639 (83)	318 (1539), 640 (88)	316 (1621), 334 (1149), 636 (99)
THF		312 (2082), 686 (71)	318 (2476), 696 (63)

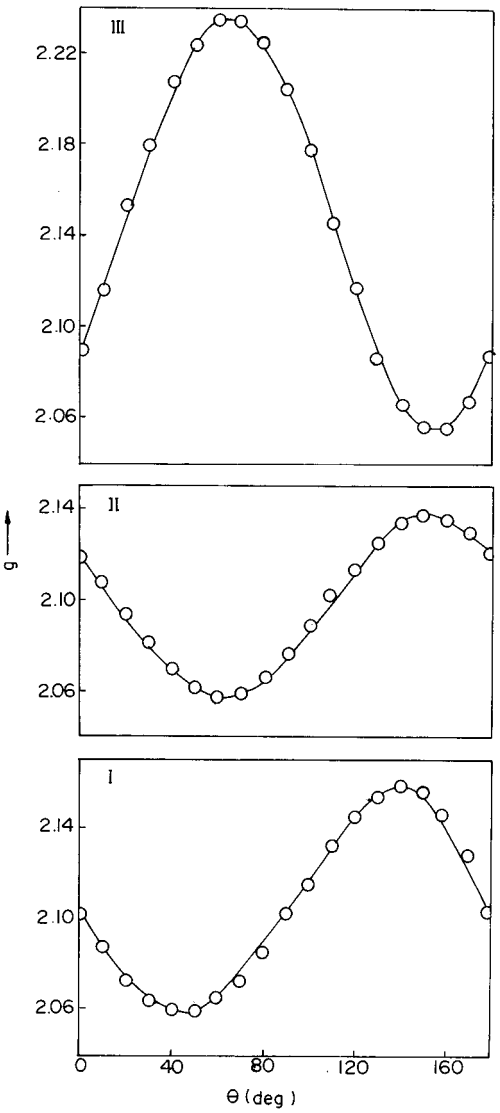

Figure 5. Angular variation of g in three orthogonal planes I, II, and III for [Cu(L-phe)(bpy)(H_2O)]ClO_4 (**2**).

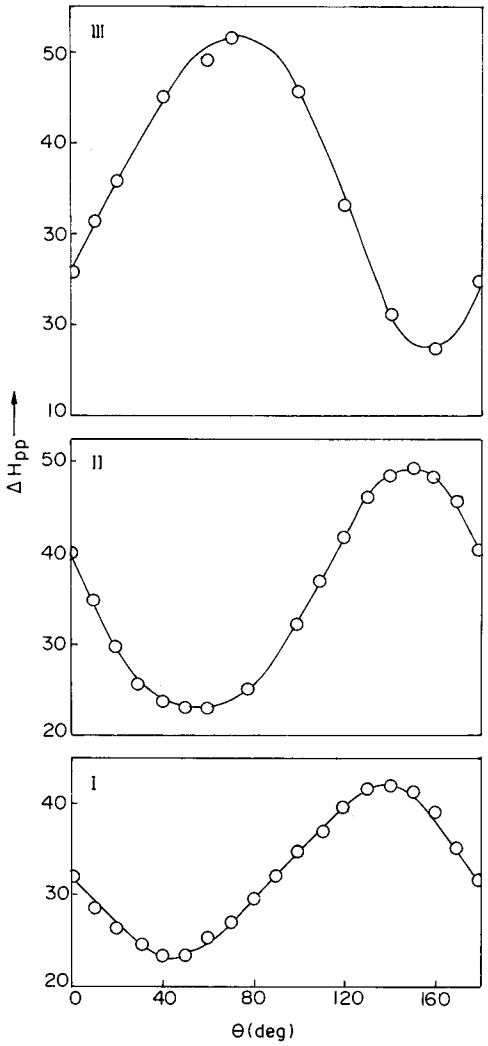

Figure 6. Angular variation of peak to peak line width (ΔH_{pp}, in G) in three orthogonal planes I, II, and III for [Cu(L-phe)(bpy)(H_2O)]ClO_4 (**2**).

dipolar contribution of about 320 G. A low value of ΔH_{pp} (16.4−51.6 G) for **2** suggests that exchange is the more dominating interaction.

Complexes **2** and **3** in CH_3CN, at 298 K, showed four resolved, equally spaced, copper hyperfine features typical of non-interacting monomeric Cu(II) species. The resonances exhibited m_I dependent line widths. The low-field hyperfine resonance was broader (46.7 G) than the high-field resonance (41.3 G), and the intensity of the hyperfine signals increased gradually in increasing field direction. In strongly coordinating solvents this difference in intensity is more visible. DMF solutions of **2** and **3** showed seven superhyperfine signals on the high-field hyperfine resonance. These features arise due to interaction of the electron spin ($S = {}^1/_2$) with the nuclear spin of three equivalent nitrogen nuclei ($I = 1$) of the coordinating bpy and L-phe ligands. The superhyperfine structure is partly resolved in CH_3OH and pyridine solvents; CH_3CN solutions did not show these features. The isotropic spin Hamiltonian parameters (g_{iso}, A_{iso}(Cu), and A_{iso}(N)) obtained after spectral simulations are listed in Table 4. These parameters are sensitive to the solvent.

In frozen solutions of **2** three of the four parallel hyperfine features were well separated while the fourth one overlapped with the perpendicular features (Figure 7). The superhyperfine

Table 4. EPR Spin Hamiltonian Parameters of [Cu(L-phe)(phen)(H_2O)]ClO_4 (**1**), [Cu(L-phe)(bpy)(H_2O)]ClO_4 (**2**), and [Cu(L-his)(bpy)]ClO_4·1.5H_2O (**3**)

complex	state[a]	temp/K	g_{iso}	A_{iso}/G	A_{iso}^N/G	$g_{\|\|}$	$g_\perp$	$A_{\|\|}$/G	$A_\perp$/G	$A_{\|\|}^N$/G
1	pc	298/77				2.238	2.056	NR	NR	
2	pc	298/77				2.236	2.056	NR	NR	
	CH_3CN	298	2.115	78.8	NR					
		77				2.235	2.058	184.9	25.7	12.9
	CH_3OH	298	2.122	80.0	10.7					
		77				2.237	2.053	183.2	22.0	12.9
	DMF	298	2.120	73.2	10.5					
		77				2.234	2.050	184.0	17.8	12.2
	pyridine	298	2.126	73.2	10.5					
		77				2.240	2.054	176.5		10.9
3	pc	298/77				2.122[c]	2.122[c]	NR	NR	NR
	CH_3CN	298	2.127	63.1	9.5					
		77				2.101[c]	2.101[c]	NR	NR	NR
	C_2H_5OH	298	2.132	65.8	9.5					
		77				2.234	2.058	161.2	NR	NR
	DMF	298	2.126	64.8	9.5					
		77				2.239	2.062	168.0	13.2	9.5
	pyridine	298	2.125	66.0	10.5					
		77				2.254	2.060	175.5	11.5	12.8

[a] Polycrystals. [b] Not resolved. [c] Isotropic signal.

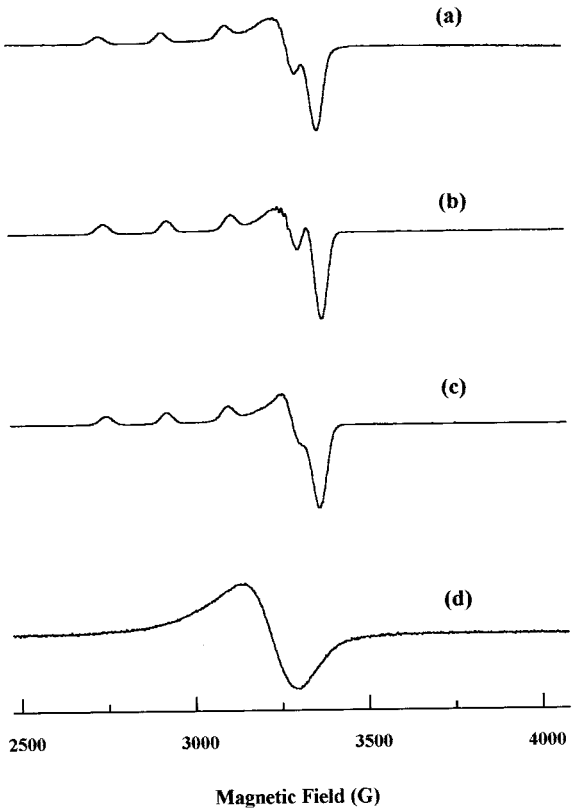

Figure 7. EPR spectra for frozen solutions of [Cu(L-phe)(bpy)(H_2O)]-ClO_4 (**2**) at 77 K: (a) CH_3OH, (b) DMF, (c) pyridine, and (d) CH_3CN.

structure was better resolved in alcohol, DMF, and pyridine solvents. In CH_3CN, the signals were relatively broader (Figure 7d). Except in CH_3CN, in the rest of the solvents complex **3** showed spectra similar to that of **2**. Interestingly, a broad isotropic resonance at $g_{iso} = 2.10$ was observed in CH_3CN. This suggests that the dimeric molecular association is retained in noncoordinating solvents like CH_3CN. However, in coordinating solvents (alcohol, DMF, and pyridine) the association is disturbed/weakened due to solvolysis or solvent coordination. The spin parameters for frozen solutions are also listed in Table 4.

Variable-Temperature ^{1}H NMR Spectra. The ^{1}H NMR spectra of complexes **1** and **2** in D_2O were measured in the temperature range 295−333 K. The complexes exhibited paramagnetic shifts due to the interaction of Cu(II) electron spin ($S = {}^1/_2$) with the nuclear spin of protons ($I = {}^1/_2$). The ^{1}H NMR signals due to phen/bpy and the phenyl group of L-phe were broad at 295 K. A shift in the resonance position and a decrease in line width were observed with increasing temperature. The signals due to inequivalent protons of bpy/phen were resolved above 323 K, but the proton spin−spin coupling could not be resolved. The signals in the chemical shift region 7.24−8.96 δ are due to the protons of phen/bpy. The broad signal at 15 δ corresponds to the phenyl group, and the sharp signal in the region 2.1−3. 4 δ is due to methylene protons. Signals due to C12H could not be detected perhaps due to proximity to the paramagnetic metal center. Representative ^{1}H NMR spectra of complexes **1** and **2** as a function of temperature are shown in Figure 8, panels a and b, respectively. The ^{1}H chemical shifts are listed in Table 5. Complex **3**, on the other hand, showed very broad signals and yielded no further information.

Proton Spin−Lattice Relaxation Studies. The spin−lattice relaxation studies of paramagnetic molecules provide information about structural dynamics. Generally, organic ligands show spin−lattice relaxation times (T_1) of the order of 1−10 s or longer, but complexes **1** and **2** have, surprisingly, shorter T_1 values. The shortest T_1 values, in the range 200−624 ms, were observed at 296 K. The relaxation time increased gradually with increasing temperature and became of the order of seconds. These values at different temperatures for **1** and **2** are listed in Table 5 along with the chemical shift parameters. T_1 values decreased gradually with an increase in electron−nuclear distance (r_{IS}). Pyridyl protons of phen/bpy have the shortest T_1 values, the methylene protons have the intermediate values, and the phenyl protons of L-phe have the largest T_1 value. The relaxation times of corresponding groups are in general shorter in **2** than in **1**.

Molecular Modeling and Conformational Isomerism. Molecular modeling studies on **2** revealed minimum energy for the "folded" (A) and "extended" (B) conformations. Structures of these minimum energy conformations are shown in Figure 9. Molecules (A or B) can be in either the *R* or *S* enantiomorph. Among these the R-form has minimum energy. Keeping the geometry as "folded" or "extended", the phenyl ring was rotated by varying the dihedral angle containing atoms C12−C13−C14−C15 and single-point strain energies were calculated. The

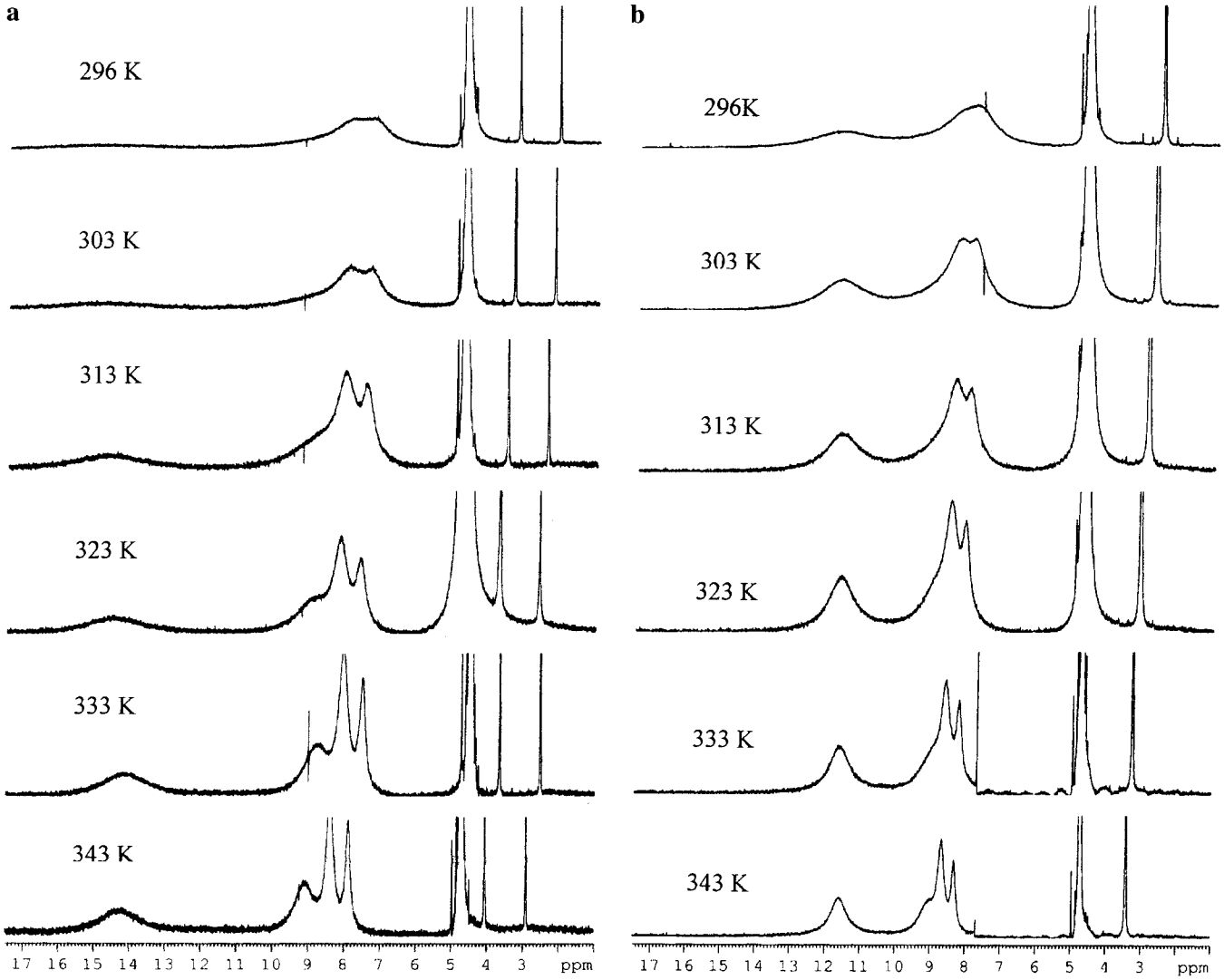

Figure 8. Variable-temperature ^{1}H NMR spectra of (a) [Cu(L-phe)(phen)(H_2O)]ClO_4 (**1**) and (b) [Cu(L-phe)(bpy)(H_2O)]ClO_4 (**2**) in D_2O.

Table 5. ^{1}H Chemical Shifts (ppm) and Spin−Lattice Relaxation Times (in Parentheses (s)) of [Cu(L-phe)(phen)(H_2O)]ClO_4 (**1**) and [Cu(L-phe)(bpy)(H_2O)]ClO_4 (**2**) in D_2O

	complex **1**			complex **2**		
		L-phe			L-phe	
temp (K)	phen	CH_2	phenyl	bpy	CH_2	phenyl
296	7.24, 7.89 (0.204)	2.11 (0.624)	15.0	7.20 (0.276)	2.58 (0.276)	11.77
303	7.39, 8.07 (2.3)	2.29 (0.729)	14.85	7.99, 8.29	2.77 (0.369)	11.67
313	7.49, 8.10	2.45	14.48	8.00, 8.46 (2.43)	2.96 (0.670)	11.65 (0.664)
323	7.63, 8.19, 8.96, 2.62 (2.45)	2.62 (1.18)	14.70	8.11, 8.51 (0.302)	3.11 (1.83)	11.64
333	7.72, 8.29, 9.06 (2.50)	2.78 (1.59)	14.29	8.22, 8.59, 8.99	3.27 (0.679)	11.64
343	8.23, 8.96	2.75	14.05	8.33, 8.69, 8.98	3.43 (0.771)	11.59

strain energy of each conformer (A or B) as a function of dihedral angle is shown in Figure 10. The calculations revealed minimum energy for the structures when the phenyl ring was parallel to the molecular plane in the case of the "folded" (A) conformation and perpendicular in the case of the "extended" (B) conformation. These results are in excellent agreement with the X-ray crystal structure of complex **2**. The difference in the total energy of folded (A) and extended (B) structures is 10.3 kcal (Table 6). Depending on the preparation conditions the complex can crystallize with either or both of the conformations. The *R* form of "folded" and the *S* form of "extended" conformations have minimum energy. But in the solid state, as revealed by the X-ray structure, the "folded" (A) form of **2** is an *S* enantiomorph. The "extended" (B) conformer crystallizes in the *S* form as predicted from theoretical study. The difference in the "folded" structure is perhaps due to intramolecular stacking and H-bonding interactions. Mullikan population analysis has revealed a difference in charge density at the Cu

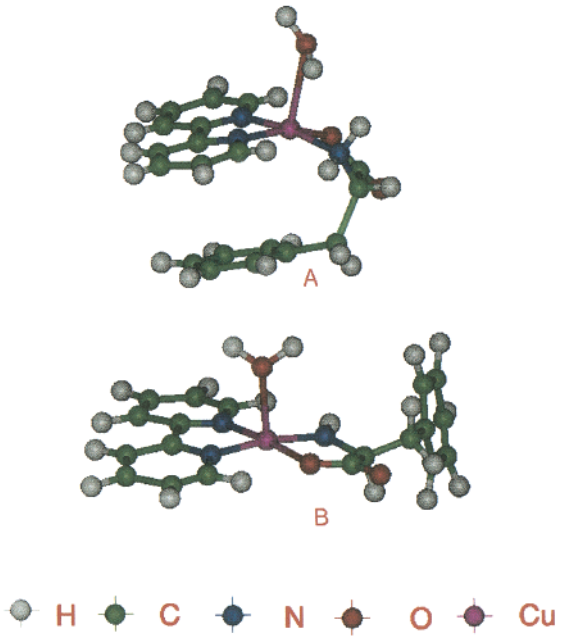

Figure 9. Minimum energy (A) "folded" and (B) "extended" conformations of [Cu(L-phe)(bpy)(H_2O)]ClO_4 (**2**) obtained from theoretical calculations.

Table 6. Total Energy, Charge Density, and HOMO−LUMO Band Gap Evaluated from DFT Calculations for [Cu(L-phe)(bpy)(H_2O)]ClO_4 (**2**)

conformation	total energy (au)	charge density	band gap (kcal/mol)
"folded" (A) *S* form	−2754.50	+1.38	18.81
"folded" (A) *R* form	−2754.52	+1.52	31.35
"extended" (B) *S* form	−2754.49	+1.42	31.35
"extended" (B) *R* form	−2754.51	+1.49	12.50

site in different conformers. The charge density is more for the "extended" *R* conformer (+1.49) than for the "folded" *S* conformer (+1.38) while the band gap energy between the HOMO and LUMO orbitals is more (by 6.3 kcal) for the "folded" *S* conformer than for the "extended" *R* conformer (Table 6). In other words, the theoretical studies while complementing the X-ray structural results suggest that complex **2** exhibits conformational isomerism.

Discussion

Single-crystal X-ray structures revealed that copper has a tetragonally elongated square pyramidal geometry. The coordination base with N_3O donor atoms is almost a perfect plane in complex **2** while it is distorted with a tetrahedral bias in **3**. Copper is out of the best N1N2N3O1 plane by 0.220 Å in **2** and by 0.271 Å in **3**. The metal−axial ligand bond is relatively weaker in **2** (Cu1−O1w = 2.298(7) Å) than in 3 (Cu1−N4 = 2.114(6) Å). Complex **2** exhibits conformational isomerism. The aromatic side chain of L-phe in **2** adopts either a "folded" (A) or an "extended" (B) conformation. In the former the phenyl group is almost coplanar with the coordination plane CuN1N2N3O1 while in the latter conformation it is almost perpendicular to the coordination plane. The crystal structure of the "folded" conformation (A) of **2** is reported in the present study while the structure of the "extended" conformation (B) was reported earlier by Sugimori et al.[14] Molecular modeling and DFT calculations have revealed that the energy difference between these two conformations is 10.3 kcal. Depending on the preparation method and conditions either of the conformational isomers can be crystallized. The "folded" (A) and "extended" (B) structures are differed in molecular interactions and association. Both intra- and intermolecular $\pi-\pi$ and H-bonding interactions stabilize the former structure while intermolecular interactions alone contribute to the stabilization of the latter structure. Complex **3** which has a side chain imidazole ring adopts a "folded" conformation, but due to the Cu−N4 bond the imidazole ring orients perpendicular to the coordination plane. Otherwise, the theoretical studies (Figure 10) reveal minimum strain energy for a parallel orientation of the aromatic ring system in the "folded" (A) conformation and a perpendicular orientation in the "extended" (B) conformation. In fact, the structures of ternary copper(II) complexes with the L-phe ligand reported so far possesses only these two conforma-

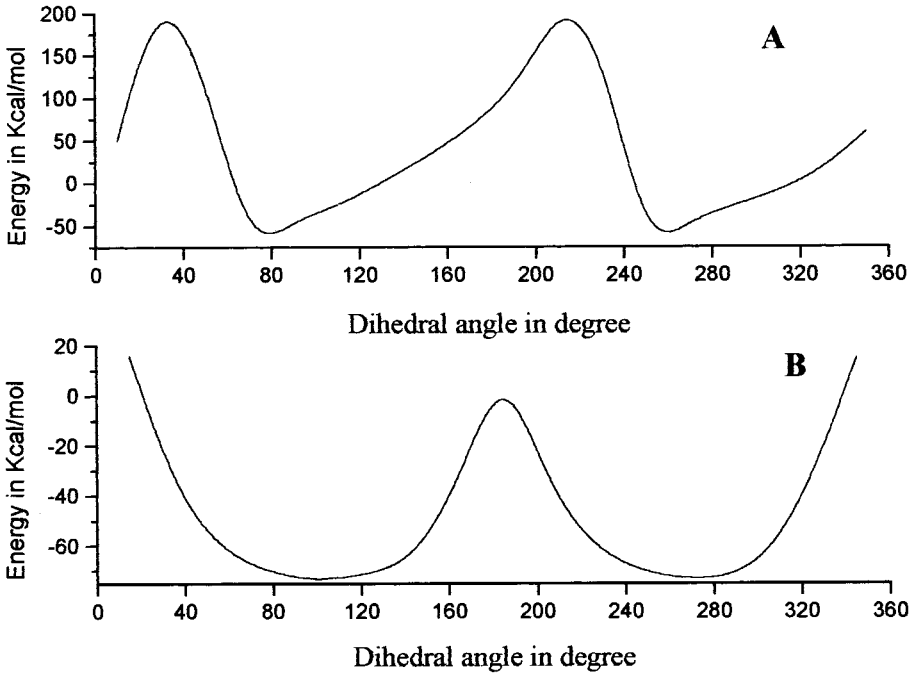

Figure 10. Strain energy as a function of dihedral angle for extended (top) and folded (bottom) conformations.

tions.[14,23] The theoretical calculations have also revealed that the *S* enantiomer has lower energy than the *R* enantiomer. However, we find some discrepancy in "folded" geometry of complex **2** wherein the structure is stabilized in an *R* enantiomeric form. We rationalize this discrepancy between the experimental and theoretical results as due to molecular stacking interactions which could not be considered in theoretical simulations. The strong inter- and intramolecular interactions perhaps lowed the energy of the *R* enantiomer of the "folded" conformation.

Interestingly, complexes **1** and **2** are amenable to both EPR and ^{1}H NMR studies. EPR spectra of pure solids showed no resolution of metal hyperfine coupling features. As described before, this is mainly due to dipolar and exchange interactions.[24] The peak to peak line width of 52 G as compared to an expected value of 320 G for purely dipolar interaction suggests that exchange overrides the dipolar interaction in complexes **1** and **2**. In an another study, one-dimensional Cu(II)−Schiff base complexes exhibited line widths of 175 G, and we have found that both dipolar and exchange interactions contribute to the line width in those complexes.[12] However, in the present complexes the exchange dominates the dipolar interaction, resulting in exchange-narrowed EPR signals of line widths in the range 16−52 G. Complex **3** showed spectra typical of weak dimeric interactions. The weak signals at 2790 and 3515 G are the two allowed perpendicular components of $\Delta m_S = \pm 1$ transitions while the signal in the low-field side at 1625 G is the half-field forbidden $\Delta m_S = \pm 2$ transition. The separation between the allowed transitions is zero-field splitting (D_{total}). This, in general, has contribution from exchange (D_{ex}) and dipole−dipole interaction (D_{dip}) terms. The latter interaction can be related to the distance (r) between the interacting Cu(II) centers as follows:

$$D_{dip} = g_{eff}{}^2\beta^2/r^3 \qquad (3)$$

Assuming $D_{ex} = 0$ and $g_{eff} = 2.122$, we estimate a value of 3.005 Å for the intermolecular Cu−Cu separation. But, according to the X-ray structure, the Cu−Cu separation is 3.811 Å. Hence, in the present case the exchange interaction term (D_{ex}) is nonzero and contributes to the zero-field splitting parameter (D_{total}). The dimeric association of **3** is present also in weakly coordinating solvents.

Much has been reported on the exchange interactions in dimeric paramagnetic complexes bridged through mono- and multiatomic ligands.[5−8] However, studies on magnetic exchange though weak molecular interactions such as $\pi-\pi$ stacking and H bonding are scarce.[9−12] The present complexes have the noteworthy result that the magnetism is primarily via weak intermolecular interactions. Exchange interaction is stronger in complex **3** than in **2**. This is mainly due to the difference in intramolecular stacking interaction and Cu−Cu separation. The $\pi-\pi$ stacking interaction is stronger in **3** than in **2** (stacking distance is only 3.66 Å in **3** while it is 4.03 Å in **2**). Additionally, the molecules are oriented in such a way that intramolecular Cu−Cu separation is shorter (3.81 Å) in **3** than in **2** (7.14 Å). The present study therefore reveals that the molecular stacking and H-bonding interactions not only stabilize the supramolecular architecture but also are responsible for the cooperative phenomenon. Such a molecular phenomenon is known in biological systems. This is also a prerequisite for molecular based sensor materials.

NMR of mononuclear copper complexes is limited due to very broad and poorly resolved signals as a consequence of rapid nuclear spin relaxation induced by the paramagnetism.[25,26] Generally, those complexes which are amenable for EPR are no good for NMR studies.[12] Recently we have found that Cu(salEen)$_2$ClO$_4$ is suitable for both EPR and NMR studies. The line width of the ^{1}H NMR signals of Cu(salEen)$_2$ClO$_4$ was sensitive to the solvent. The signals were narrow in noncoordinating or weakly coordinating $CDCl_3$ and CD_3CN solvents and broad in D_2O. This was rationalized due to a change in the molecular geometry of copper from a distorted square planar to a square pyramidal due to solvent coordination. The present study confirms our earlier observations. The ^{1}H NMR signals of complexes **1** and **2** in D_2O were broad while those of **3** were much broader. This is consistent with the square pyramidal structure of the copper complexes. The line width of ^{1}H NMR signals for **1** and **2** decreased with increasing temperature (Figure 8) while that of **3** was invariant. This difference is because of structural dynamics in complexes **1** and **2** which is absent in **3**. As evident from the single-crystal X-ray structures and molecular modeling studies, complexes **1** and **2** possess either a "folded" (A) or an "extended" (B) conformation. The difference in energy between these two conformation is 10.3 kcal. At higher temperatures a conversion between these two conformations is possible. The structural dynamics at higher temperatures is responsible for the resolution and lower line width of the ^{1}H NMR signals. As the side chain containing the imidazole group of L-his is involved in coordination with copper, it is not possible for **3** to exhibit such a structural dynamics. Generally T_1 of protons in paramagnetic complexes is of the order of milliseconds. Complexes **1** and **2** exhibited higher T_1 values at higher temperatures. This is due to the conformational dynamics in **1** and **2** at higher temperatures.

UV−vis data in different solvents suggest that the coordination geometry of copper is sensitive to the donor capacity of the solvent. Copper expands its coordination number from 5 to 6 in strong donor solvents. This can be inferred from the red shift in the d−d band position from 580 to 690 nm. When copper becomes hexacoordinated, the molecule changes its conformation from a "folded" to an "extended" geometry. This facile structural transformation of copper is responsible for its reactivity in metalloenzymes. The conformational change (from a "folded " to an "extended" conformation) modulates the electron density, charge distribution, and redox behavior of copper. As apparent from Table 6 the charge on copper is lower for an "extended" (*S*) conformation than for a "folded" (*S*) conformation. In otherwords, nucleophillic attack is favored in an "extended" (*S*) conformation while electrophillic attack is favored in a "folded" (*S*) conformation. These facile structural and electronic changes have been realized to be responsible for the reactivity of copper in metalloenzymes.

Conclusions

Three ternary copper(II) complexes, [Cu(L-phe)(phen)(H_2O)]ClO$_4$ (**1**), [Cu(L-phe)(bpy)(H_2O)]ClO$_4$ (**2**), and [Cu(L-his)(bpy)]ClO$_4$·1.5H_2O (**3**), were synthesized and characterized by single-crystal X-ray and spectroscopic (FT-IR, UV−vis, EPR, and ^{1}H NMR) techniques. Complexes **1** and **2**, in the solid state, form supramolecular networks via weak intra- and intermolecular $\pi-\pi$ stacking and H-bonding interactions, while **3** exists as weak dimers. Complexes **1** and **2** exhibit conformational

(25) . *NMR of Paramagnetic Molecules: Principles and Applications*; La Mar, G. N., Horrocks, W. DeW., Jr., Holm, R. H., Eds.; Academic Press: New York, 1973.
(26) Bertini, I., Luchinat, C. *NMR of Paramagnetic Molecules in Biological Systems*; Benjamin & Cummings: Menlo Park, CA, 1986.

isomerism. The phenyl side chain of L-phe adopts either a "folded" (A) or an "extended" (B) conformation. ^{1}H NMR studies in D_2O reveal an interconversion between A and B conformers at high temperatures (>323 K). Single-crystal EPR studies reveal that the weak molecular interactions are the pathways for magnetic exchange. Complexes **1** and **2** belong to the class of a few paramagnetic copper(II) complexes amenable to both EPR and ^{1}H NMR studies. These complexes also belong to the category of limited reported systems exhibiting magnetism through weak molecular interactions. The tetragonally elongated square pyramidal geometry of copper, the capacity to expand the coordination number from 5 to 6 in strong donor solvents (as revealed by UV−vis spectroscopy), and the self-organization and three-dimensional magnetic behavior via weak molecular interactions are the salient features of the present complexes.

Supporting Information Available: X-ray crystallographic files in CIF format. This material is available free of charge via the Internet at http://pubs.acs.org.

IC010182D